Journal Pre-proof

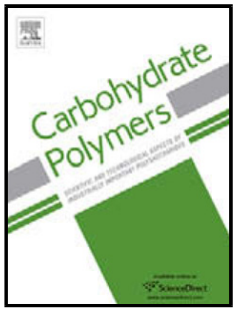

Conductive polysaccharides-based proton-exchange membranes for fuel cell applications: The case of bacterial cellulose and fucoidan

Carla Vilela, Ana C.Q. Silva, Eddy M. Domingues, Gil Gonçalves, Manuel A. Martins, Filipe M.L. Figueiredo, Sónia A.O. Santos, Carmen S.R. Freire

PII: S0144-8617(19)31272-X

DOI: https://doi.org/10.1016/j.carbpol.2019.115604

Reference: CARP 115604

To appear in: *Carbohydrate Polymers*

Received Date: 30 September 2019

Revised Date: 28 October 2019

Accepted Date: 9 November 2019

Please cite this article as: { doi: https://doi.org/

Conductive polysaccharides-based proton-exchange membranes for fuel cell applications: the case of bacterial cellulose and fucoidan

Carla Vilela[a*] cvilela@ua.pt, Ana C. Q. Silva[a], Eddy M. Domingues[b], Gil Gonçalves[c], Manuel A. Martins[d], Filipe M. L. Figueiredo[b], Sónia A. O. Santos[a], Carmen S. R. Freire[a]

[a] CICECO – Aveiro Institute of Materials, Department of Chemistry, University of Aveiro, 3810-193 Aveiro, Portugal.

[b] CICECO – Aveiro Institute of Materials, Department of Materials and Ceramic Engineering, University of Aveiro, 3810-193 Aveiro, Portugal.

[c] Centre for Mechanical Technology and Automation (TEMA), Department of Mechanical Engineering, University of Aveiro, 3810-193 Aveiro, Portugal.

[d] CICECO – Aveiro Institute of Materials, Department of Physics, University of Aveiro, 3810-193 Aveiro, Portugal.

[*] Corresponding author: C. Vilela

Graphical abstract

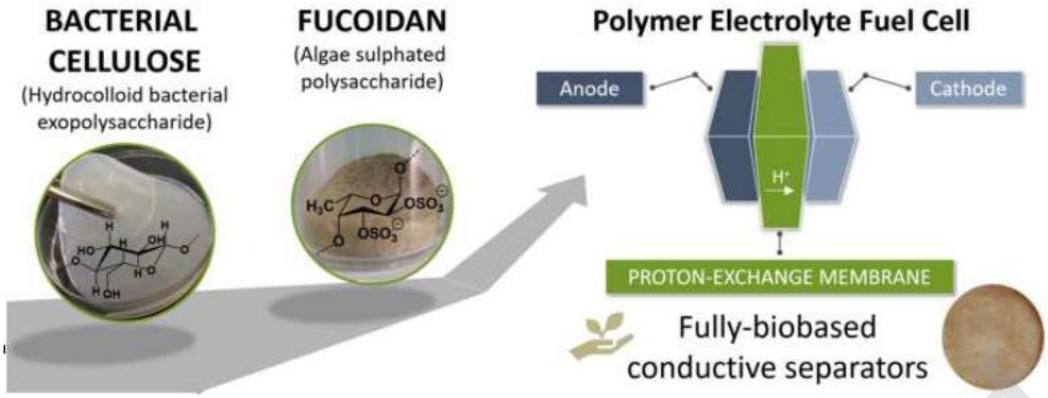

Highlights

- Fully bio-based membranes composed of bacterial cellulose (BC) and fucoidan.
- Nanostructured membranes with thermal-oxidative stability in the range 180–200 °C.
- Membranes with good dynamic mechanical performance (storage modulus ≥ 460 MPa).
- BC/fucoidan proton-exchange membranes with protonic conductivity of 1.6 mS cm^{-1}.
- Conductive bio-based separators for application in polymer electrolyte fuel cells.

Abstract

Conductive natural-based separators for application in polymer electrolyte fuel cells (PEFCs) were fabricated by combining a bacterial polysaccharide, *i.e*. bacterial cellulose (BC), and an algae sulphated polysaccharide, *i.e*. fucoidan (Fuc). The diffusion of fucoidan aqueous solution containing a natural-based cross-linker, *viz*. tannic acid, into the wet BC nanofibrous three-dimensional network, followed by thermal cross-linking, originated fully bio-based proton exchange membranes (PEMs). The PEMs present thermal-oxidative stability in the range of 180–200 °C and good dynamic mechanical performance (storage modulus ≥ 460 MPa). Additionally, the BC/Fuc membranes exhibit protonic conductivity that increases with increasing relative humidity (RH), which is a typical feature for numerous water-mediated proton conductors. The traditional Arrhenius-type plots demonstrate a linear behaviour with a maximum protonic conductivity of 1.6 mS cm^{-1} at 94 °C and 98% RH. The results showed that these fully bio-based conductive membranes have potential as eco-friendly alternatives to other PEMs for application in PEFCs.

Keywords: bacterial cellulose, fucoidan, proton-exchange membranes, protonic conductivity, fully bio-based separators

1. Introduction

The development of environmentally friendly materials derived from renewable resources as surrogates of fossil-based counterparts is one of the goals of the 2030 Agenda for Sustainable Development in the attempt to curb pollution and climate change. Therefore, natural occurring polymers, such as polysaccharides and proteins (Silva et al., 2014; Vilela, Pinto, et al., 2018), are major players to design innovative

eco-friendly materials with customizable properties and performance. One of the polysaccharides that is contributing at a fast pace to engineer multifunctional bio-based materials, is cellulose, and more specifically its nanoscale forms, namely cellulose nanofibrils (CNFs), cellulose nanocrystals (CNCs) and bacterial cellulose (BC) (Klemm et al., 2018). While the first two nanocelluloses are commonly extracted from plant cellulose by mechanical, chemical or enzymatic methodologies (or a combination of those) (Thomas et al., 2018), the third nanocellulose form is biosynthesized by non-pathogenic gram-positive and gram-negative bacteria (Wang, Tavakoli, & Tang, 2019).

The intrinsic properties of the hydrocolloid bacterial exopolysaccharide BC, namely high purity, *in situ* moldability (*i.e*. ability to be biosynthesized in the form of membranes or films with customizable size and form) and shape retention (Silvestre, Freire, & Neto, 2014; Wang et al., 2019), are what differentiates it from the other two nanocellulose counterparts. This set of properties, together with its dimensional stability, porous structure, water-holding capacity, first-rate mechanical properties and tunable surface chemistry, enables its use in the pure form, after chemical or physical modification, or after combination with organic and inorganic compounds to design composites or hybrid materials with specific functionalities (Foresti, Vázquez, & Boury, 2017; Torgbo & Sukyai, 2018; Torres, Arroyo, & Troncoso, 2019). In fact, the aptitude of BC to harbour diverse molecules and macromolecules within its ultrafine nanofibrous network originates functional nanomaterials with properties that are not inherent to this exopolysaccharide, like for instance, ionic conductivity (Gao-peng Jiang et al., 2015; Gaopeng Jiang, Qiao, & Hong, 2012; Vilela, Martins, et al., 2018; Vilela, Moreirinha, Domingues, et al., 2019). This property has proven to be particularly important in the context of ion-exchange membranes for application as proton-conducting separators in

polymer electrolyte fuel cells (PEFCs) (Vilela, Silvestre, Figueiredo, & Freire, 2019), whose research is being directed towards the production of natural-based membranes.

Under the premises of the sustainable development goals, the use of BC in tandem with a water-soluble polysaccharide containing protogenic groups, *e.g*. sulphate groups ($-SO_4^-$) that enable proton motion, is a promising and eco-friendly route to design fully bio-based proton-exchange membranes (PEMs). An example of such type of compounds includes the k-carrageenan extracted from red seaweed that, after blending with 1-butyl-3-methyl-1H-imidazolium chloride ([Bmim]Cl) ionic liquid and glycerol, was tested as electrolyte in fuel cells (Nunes et al., 2017). Fucoidan is another example of a sulphated polysaccharide found in diverse species of brown algae, but that is particularly abundant in *Fucus vesiculosus* (Zayed & Ulber, 2019). This anionic algae sulphated polysaccharide is mostly composed of fucose and sulphate, albeit small proportions of other monosaccharides (*e.g*., mannose, galactose, glucose and xylose), uronic acids or even acetyl moieties may also be present (Catarino, Silva, & Cardoso, 2018). Fucoidan is primarily explored for its manifold biological activities, namely anti-oxidant, anti-inflammatory, anti-coagulant, anti-thrombotic, anti-viral and anti-cancer activities (Luthuli et al., 2019; Wang et al., 2019; Weelden et al., 2019; Zayed & Ulber, 2019). Nevertheless, this sulphated polysaccharide is also being exploited for its polyelectrolytic nature that enables, for instance, the design of polyelectrolyte complexes (Lee & Lim, 2014) or multilayer structures (Ho et al., 2015; Webber, Benbow, Krasowska, & Beattie, 2017). As for the aforementioned example of k-carrageenan (Nunes et al., 2017), fucoidan also has potential for the development of ion-conducting separator materials for application in PEFCs or other electrochemical and energy-conversion devices involving functional ion-conducting elements. However, and since a PEFC produces water and heat as reaction products, there is the obvious

limitation of the water solubility of fucoidan for this type application. Therefore, this sulphated polysaccharide must be chemically or physically modified in order to be used as a solid polymer electrolyte in fuel cells.

Herein, the unprecedented combination between BC (the support), fucoidan (the polyelectrolyte) and tannic acid (the cross-linker) was studied as a strategy to develop a fully bio-based PEM for application in PEFCs. Fucoidan was extracted from *F. vesiculosus* by microwave-assisted extraction and incorporated into a wet BC membrane via the simple diffusion of an aqueous solution of the sulphated polysaccharide (and tannic acid as natural cross-linker) into the bacterial polysaccharide three-dimensional network, followed by thermal cross-linking. The composition, microstructure, thermal and oxidative stability, dynamic mechanical properties, moisture-uptake capacity and protonic conductivity was investigated, and their relationship discussed.

2. Experimental

2.1. Chemicals and materials

Citric acid ($C_6H_8O_7$, ≥99.5%), glucose ($C_6H_{12}O_6$, ≥99.5%), potassium sulphate (K_2SO_4, ≥99.0%), sodium phosphate dibasic (Na_2HPO_4, ≥99.0%) and tannic acid ($C_{76}H_{52}O_{46}$, source: Chinese natural gall nuts) were purchased from Sigma-Aldrich (Sintra, Portugal). Bacteriological agar, peptone and yeast extract were purchased from Himedia Laboratories GmbH (Einhausen, Germany). Ultrapure water (Type 1, 18.2 MΩ·cm at 25 °C) was purified by a Simplicity® Water Purification System (Merck, Darmstadt, Germany). Other chemicals and solvents were of laboratory grades.

Fucus vesiculosus was collected from a salt river near Aveiro (Portugal) in January 2014. Prior to use, the seaweed was thoroughly washed under fresh tap water to remove

sand and epiphytes, dried at 40 °C in a vacuum drying oven (Thermo Fisher Scientific, Massachusetts, USA) and milled in an electric grinder (Moulinex A980, France). Then, the milled seaweed was washed with a solvent mixture (1 g *per* 20 mL) of chloroform and methanol (2:1 v/v) under stirring for 20 min, centrifuged at 2500 rpm during 20 min, dried at 40 °C in a vacuum drying oven, and stored in a desiccator at room temperature (RT) until further use.

2.2. Bacterial cellulose (BC) biosynthesis

BC consisting of a three-dimensional network of nano- and microfibrils with 10–200 nm width was biosynthesized in our laboratory in the form of wet membranes using the *Gluconacetobacter sacchari* bacterial strain (Trovatti, Serafim, Freire, Silvestre, & Neto, 2011). Briefly, the bacteria were incubated in a Hestrin-Schramm (HS) liquid medium (20 g L^{-1} glucose, 5 g L^{-1} peptone, 5 g L^{-1} yeast extract, 2.7 g L^{-1} Na_2HPO_4, 1.15 g L^{-1} citric acid, and 15 g L^{-1} agar, pH 5) under static conditions. After incubation at 30 °C during several days, the BC membranes were separated from the media, treated with 0.5 M NaOH aqueous solution to eliminate cells attached to the matrix and repeatedly washed with ultrapure water to remove culture media components. Finally, the membranes were whitened with 1% sodium hypochlorite solution, washed several times with water until neutral pH, and stored in ultrapure water in the refrigerator until further use.

2.3. Fucoidan (Fuc) microwave-assisted extraction

Fucoidan was extracted from *F. vesiculosus* by microwave-assisted extraction following an established procedure (Rodriguez-Jasso, Mussatto, Pastrana, Aguilar, & Teixeira, 2011). Briefly, the milled seaweed and ultrapure water (1 g per 25 mL) were

placed in a glass vessel and irradiated in a Monowave 300 microwave apparatus (Anton Paar GmbH, Graz, Austria) during 1 min at 172 °C. After irradiation, the vessel was cooled in an ice bath and the reaction mixture centrifuged at 4000 rpm during 5 min to separate the residual seaweed. Then, an aqueous solution of $CaCl_2$ (1% w/w) was added to the liquid fraction. This mixture was kept overnight at 4 °C to precipitate the extracted alginate (*viz*. the major seaweed polysaccharide) and the cross-linked alginate was removed by filtration. The precipitation of fucoidan was promoted by adding an excess of absolute ethanol to the resultant filtrate and maintain the mixture at 4 °C during 8 h. The ethanol-precipitated polysaccharide was recovered by centrifugation (5000 rpm, 20 min, 4 °C), oven dried at 40 °C, milled in an agate mortar and stored for further analyses. The microwave-assisted extraction originated a fucoidan-enriched fraction (denominated from now on as Fuc) with an extraction yield of 11.6±4.4%. The algal polysaccharide-enriched fraction presents a sulphate content of *ca*. 5.5% determined by elemental analysis (LECO TruSpec 630-200-200 CHNS, LECO Corporation, Michigan, USA) and a zeta potential of *ca*. –15.0 mV (Zetasizer Nano ZS, Malvern Panalytical, Cambridge, United Kingdom).

2.4. Preparation of BC/Fuc membranes

Wet BC membranes with a diameter of *ca*. 75 mm and 40% water content were placed in a petri-dish containing an aqueous solution of fucoidan (50 and 75% w/w relative to BC) and tannic acid (TA, 20% w/w relative to BC), as summarized in Table 1. After the complete absorption of the corresponding solution at RT, the membranes were placed in a ventilated oven (Thermo Fisher Scientific, Massachusetts, USA) at 105 °C for 24 h to promote thermal cross-linking during the drying process. All membranes were prepared in triplicates and kept in desiccators until further use.

Table 1 Composition and thickness of the pure BC and prepared BC/Fuc membranes.

Samples	Composition [a]			Thickness / μm
	W_{Fuc}/W_{BC}	W_{Fuc}/W_{total}	W_{Fuc}/V_{total} (mg cm^{-3})	
BC	–	–	–	35±1
BC/Fuc_50	0.50	0.33	470±13	52±5
BC/Fuc_75	0.75	0.43	573±15	79±6

[a] composition was calculated by considering the dry weight of the membranes (W_{total}), BC (W_{BC}) and fucoidan (W_{Fuc}), and the volume of the membrane (V_{total}); the values are the mean of at least three replicates with the respective standard deviations.

2.5. Characterization methods

A hand-held digital micrometer (Mitutoyo Corporation, Tokyo, Japan) with an accuracy of 0.001 mm was used to measure the thickness of the membranes.

Attenuated total reflection-Fourier transform Infrared (ATR-FTIR) spectra were recorded with a Perkin-Elmer FT-IR System Spectrum BX spectrophotometer (Perkin-Elmer Inc., Massachusetts, USA) equipped with a single horizontal Golden Gate ATR cell, over the range of 600–4000 cm^{-1} at a resolution of 4 cm^{-1} over 32 scans.

X-ray photoelectron spectroscopy (XPS) spectra were acquired in an Ultra High Vacuum (UHV) system with a base pressure of 2×10^{-10} mbar. The system is equipped with a hemispherical electron energy analyser (SPECS Phoibos 150), a delay-line detector and a monochromatic Al Kα (1486.74 eV) X-ray source. High-resolution spectra were recorded at normal emission take-off angle and with a pass-energy of 20 eV. The binding energies obtained in XPS analysis were corrected with the reference to the first component of C1s core level (284.6 eV). For the XPS measurements, a drop

of the fucoidan aqueous solution was deposited on silicon substrate by drop casting and the pure BC and BC/Fuc_75 membranes were analysed as such.

Micrographs of the surface and cross-section of the membranes were obtained by an ultra-high-resolution field-emission HR-FESEM Hitachi SU-70 microscope (Hitachi High-Technologies Corporation, Tokyo, Japan) coupled with a microanalysis system Bruker QUANTAX 400 detector for energy dispersive X-ray spectrometry (EDS). The membranes for surface and cross-section (fractured in liquid nitrogen) examination were placed on a steel plate and coated with a carbon film prior to analysis.

The surface profile and roughness of the membranes were acquired with a Sensofar S neox 3D non-contact 3D optical profilometer (Sensofar, Barcelona, Spain) operating in confocal mode with a 20× magnification objective lens. The optical profiler is equipped with a black and white 1360×1024 pixels CCD sensor. The average surface roughness was determined according to ISO 25178 (S_a – arithmetical mean height of the surface; 3D areal surface texture) (Aver'yanova, Bogomolov, & Poroshin, 2017).

Thermogravimetric analysis (TGA) was carried out with a SETSYS Setaram TGA analyser (SETARAM Instrumentation, Lyon, France) equipped with a platinum cell. The samples were heated from 25 to 800 °C at a constant rate of 10 °C min^{-1} under two distinct atmospheres, namely nitrogen and oxygen (200 mL min^{-1}).

Dynamic mechanical analysis (DMA) curves of rectangular membrane pieces with 30×5 mm^2 were obtained on a Tritec 2000 DMA (Triton Technologies, London, UK) operating in tension mode (single strain) at 1 Hz and with 0.005 mm displacement. The temperature was swept from −50 to 180 °C with a constant heating rate of 2 °C min^{-1}.

The moisture-uptake capacity was assessed by placing the dry membrane specimens (20×20 mm^2) and the fucoidan powder in a conditioned cabinet at about 98% RH (saturated potassium sulphate aqueous solution, 97.59±0.53% (Greenspan, 1977)) at

RT for 48 h. After removing the specimens from the chamber, the weight (W_w) was measured and the moisture-uptake was calculated according to the equation: $Moisture\ uptake\ (\%) = (W_w - W_0) \times W_0^{-1} \times 100$, where W_0 is the initial weight of the dry membrane.

Electrochemical impedance spectroscopy (EIS, Agilent E4980A Precision LCR meter, Santa Clara, CA, USA) was used to determine the through-plane (TP) protonic conductivity (σ) under variable temperature (40 °C to 94 °C) and RH (40% to 98%) conditions in an ACS Discovery DY110 climatic chamber (Angelantoni Test Technologies Srl, Massa Martana, Italy). The measurements were performed on specimens with an area of *ca*. 10×10 mm^2 on which two circular silver paste electrodes (Agar Scientific, Essex, UK) were painted on opposite sides of the membrane. A pseudo 4-electrode configuration in a tubular sample holder was used to ensure full exposure of the membrane surface to the controlled atmosphere and provide the necessary electrical contact between the sample and the LCR meter. The impedance spectra were recorded between 20 Hz and 2×10^6 Hz with test signal amplitude of 100 mV and analysed with the ZView software (Version 2.6b, Scribner Associates, Southern Pines, NC, USA) to evaluate the Ohmic resistance (R) of the membrane. The conductivity was then calculated using the equation: $\sigma = L(RA)^{-1}$, where L is thickness of the dry membrane, and A is the area of the electrodes.

3. Results and discussion

A pair of membranes composed of two polysaccharides, *viz*. bacterial cellulose and fucoidan, with different mass ratios were prepared via the simple diffusion of a fucoidan aqueous solution containing a natural-based cross-linker into the wet BC nanofibrous three-dimensional network (Fig. 1A). BC was selected for its three-dimensional porous

structure, thermal stability and mechanical performance, whereas fucoidan was selected due to its sulphated moieties ($-OSO_3^-$) that enable proton motion. In addition, the non-toxic tannic acid (TA), from gall nuts, was used as a natural-based cross-linker to retain the water-soluble fucoidan inside the wet BC nanofibrous network (Fig. 1B). This naturally derived phenolic compound was chosen because of its ability to promote the cross-linking of neutral or charged macromolecules at diverse bonding sites via chemical and physical interactions (Chen et al., 2019; Erel-Unal & Sukhishvili, 2008; Fan et al., 2017). The resulting BC/Fuc membranes were homogenously brownish due to the algae polysaccharide enriched fraction, as depicted in Fig. 1C. Moreover, the two membranes were developed with different compositions, namely BC/Fuc_50 with 470±13 mg of fucoidan per cm^3 of membrane and BC/Fuc_75 with 573±15 mg of fucoidan per cm^3 of membrane, which translates into membranes with distinct thickness values, *viz*. 52±5 µm and 79±6 µm, respectively (Table 1).

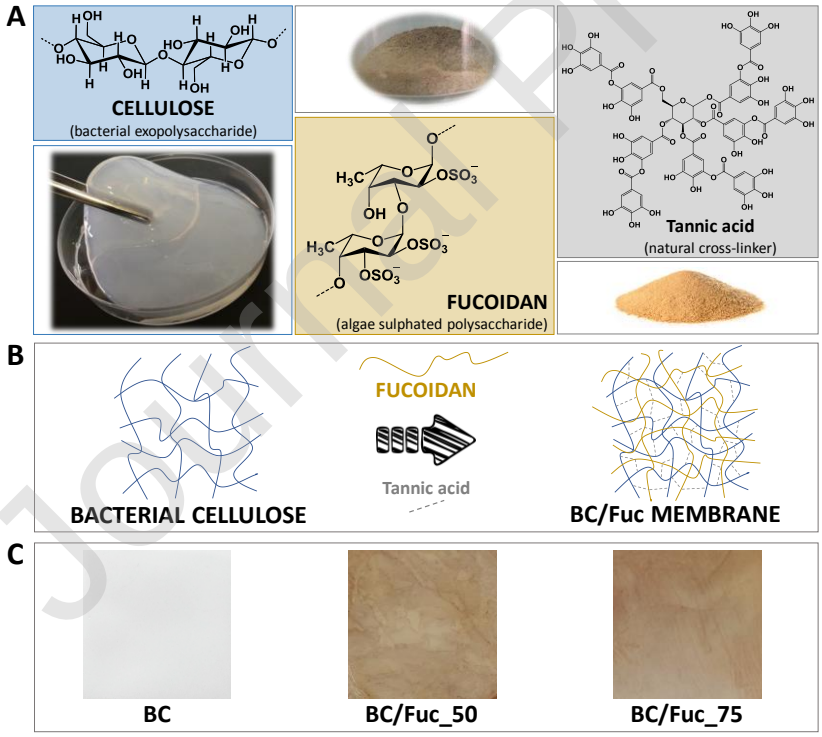

Fig. 1. (A) Chemical structure of bacterial cellulose, fucoidan from *F. vesiculosus* (Zayed & Ulber, 2019) and tannic acid, and the corresponding photographs of the wet

BC membrane, and fucoidan and tannic acid powders, (B) scheme of the route to prepare the BC/Fuc membranes, and (C) photographs of the dry BC and BC/Fuc membranes.

The BC/Fuc membranes were characterized regarding structure/composition (ATR-FTIR, EDS, XPS), morphology (HR-FESEM), topography (3D confocal profilometry), thermal-oxidative stability (TGA), dynamic mechanical performance (DMA), moisture-uptake capacity, protonic conductivity (EIS), and compared with the pristine components.

3.1. Structure and chemical composition

The structural analysis of the BC/Fuc membranes and the corresponding individual components by vibrational spectroscopy is displayed in Fig. 2. The ATR-FTIR spectrum of pure BC (Fig. 2A) presents the characteristic absorption bands of cellulose at 3341 cm^{-1} assigned to the O–H stretching vibration of the primary and secondary hydroxy groups, 2898 cm^{-1} allocated to the stretching vibration of the C–H bonds, 1315 cm^{-1} attributed to the O–H in plane bending vibration of the primary and secondary hydroxy groups, 1160 cm^{-1} assigned to the C–O–C antisymmetric stretching vibration of the glycosidic bonds, and 1031 cm^{-1} ascribed to the C–O stretching vibration (Foster et al., 2018).

The ATR-FTIR spectrum of fucoidan (Fig. 2B) exhibits the typical structural pattern of fucoidan from *F. vesiculosus* (Fig. 1A). According to literature, the structure of fucoidans is quite complex and mainly species-related, and fucoidan from *F. vesiculosus* is composed of alternating (1→3)- and (1→4)-linked α-L-fucopyranoside backbone with sulphate substituents ($-OSO_3^-$) at C-2 and alternating C-3 in the α-L-

fucopyranose residue depending on the glycosidic linkages (Ale & Meyer, 2013; Catarino et al., 2018; Weelden et al., 2019; Zayed & Ulber, 2019), as illustrated in Fig. 1A. This pattern is corroborated by the presence of an absorption band at about 1248 cm^{-1} allocated to the S=O stretching, as well as by the sharp band at around 838 cm^{-1} assigned to the C−O−S bending vibrations of the sulphate substituents (Espinosa-Velázquez, Ramos-de-la-Peña, Montanez, & Contreras-Esquivel, 2018; Pielesz & Biniaś, 2010). Furthermore, the absorption bands at 3354 cm^{-1}, 1416 cm^{-1} and 1028 cm^{-1} correspond to the O–H stretching, CH_3 symmetrical bending and C–O stretching vibrations (Bellamy, 1975), respectively; whereas the band at 1594 cm^{-1} can be attributed to the C=O stretching vibrations, since this fucoidan-enriched fraction may also contain uronic acids (Catarino et al., 2018). In fact, a previous study reported the existence of 4.9% of uronic acids in a fucoidan extracted from *F. vesiculosus* (Ho et al., 2015).

Regarding the BC/Fuc membranes, the ATR-FTIR spectra are the combination of the those of the individual components. As observed in Fig. 2C and Fig. 2D, both membranes exhibit the signature vibrations of the cellulose backbone at 3340 cm^{-1} (O–H stretching), 2900 cm^{-1} (C–H stretching), 1310 cm^{-1} (O–H bending) and 1030 cm^{-1} (C–O stretching) (Foster et al., 2018), in conjunction with the characteristic absorption bands of fucoidan at about 1240 cm^{-1} (S=O stretching) and 830 cm^{-1} (C−O−S bending) (Espinosa-Velázquez et al., 2018).

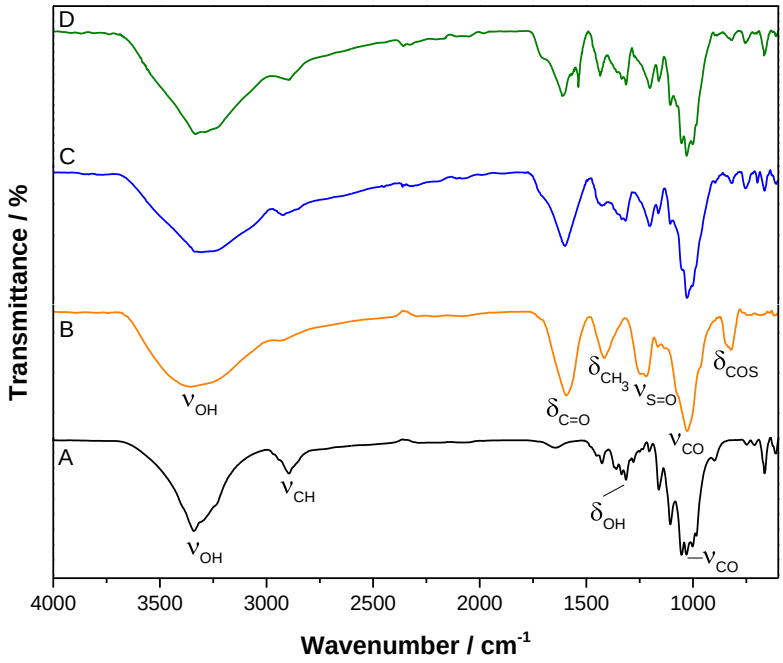

Fig. 2. ATR-FTIR spectra (vibrational modes: ν = stretching, δ = bending) of (A) pure BC, (B) fucoidan, and membranes (C) BC/Fuc_50 and (D) BC/Fuc_75.

The elemental chemical composition of the cross-sectional sections of the BC/Fuc membranes was confirmed by EDS analysis. Fig. 3 depicts the spectra of the two fully bio-based membranes that reiterate the presence of BC and fucoidan through the detection of the carbon (C), oxygen (O) and sulphur (S) peaks at 0.27, 0.51 and 2.31 keV, respectively. The semi-quantitative analysis shows that BC/Fuc_50 is composed of *ca*. 68% of C, 24% of O and 8% of S (Fig. 3B), while BC/Fuc_75 contains 66% of C, 20% of O and 14% of S (Fig. 3A). The oxygen-to-carbon (O/C) atomic ratio is 0.35 for BC/Fuc_50 and 0.30 for BC/Fuc_75, and as expected the sulphur content of BC/Fuc_75 (43 wt.% of fucoidan) is superior to that of BC/Fuc_50 (33 wt.% of fucoidan). The surface chemical composition was also checked by EDS mapping of sulphur, which conveyed a detectable amount and a uniform distribution of the element itself in both membranes, as illustrated in Fig. 3C for BC/Fuc_50 and Fig. 3D for BC/Fuc_75. From the data presented here, it is clear that the sulphated polysaccharide was successfully

incorporated into the BC porous three-dimensional network, as formerly assessed by the FTIR-ATR analysis.

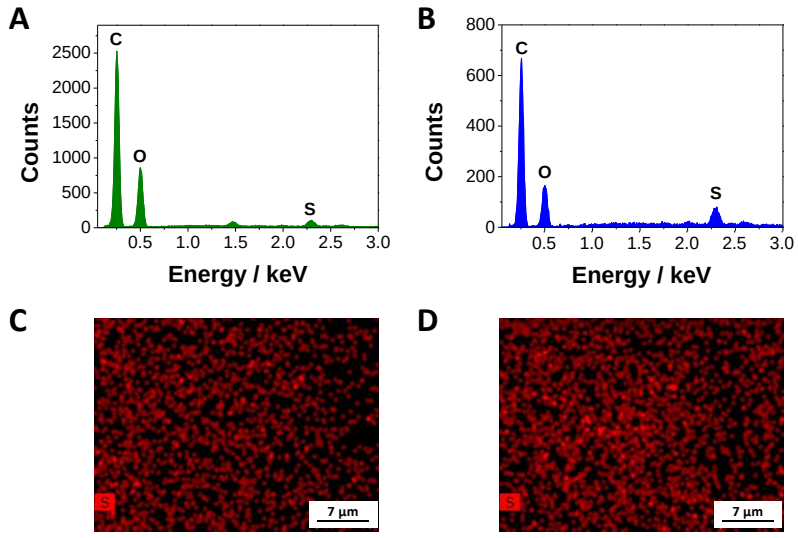

Fig. 3. EDS spectra (A and B) and mapping (C and D) of the cross-sectional surface of the membranes BC/Fuc_50 (A and C) and BC/Fuc_75 (B and D).

The chemical composition of the surface of the BC/Fuc_75 membrane was further examined by XPS. Table 2 summarizes the surface atomic concentrations and Fig. 4 depicts the XPS survey- and high-resolution spectra (C1s and S2p) of the BC/Fuc_75 membrane and the respective pure components, *viz*. BC and fucoidan. The XPS survey scan (Fig. 4A) demonstrates that carbon (C1s) and oxygen (O1s) are the dominant elements detected in all membranes at binding energies of *ca*. 285 eV and 533 eV, respectively. In the case of fucoidan and BC/Fuc_75, a peak at a binding energy of *ca*. 169 eV is also present, which is characteristic of sulphur element. The detection of minor amounts of other elements on the samples of fucoidan and BC/Fuc_75 membrane (Fig. 4A) might be associated with the fact that the sulphated polysaccharide is an enriched fraction and, hence, contains other elements, like for example calcium and sodium, as previously reported for fucoidan from *F. vesiculosus* (Ho et al., 2015).

Herein, the XPS analysis was only centred on the relative abundance of carbon, oxygen and sulphur (Table 2), while the other elements were neglected.

The XPS analysis shows that BC is composed of 62.4% of carbon and 37.6% of oxygen with a O/C atomic ratio of 0.60, which agrees with data reported in literature (Chen & Huang, 2015; Li, Wan, Li, Liang, & Wang, 2009). For fucoidan, the surface composition is consistent with the structure of this sulphated polysaccharide, composed of 60.2% of carbon, 35.7% of oxygen and 4.1% of sulphur, with O/C and C/S atomic ratios of 0.59 and 14.7, respectively. A previous study reported comparable compositional data for fucoidan from *F. vesiculosus*: 56.8% of C, 37.1% of O and 3.9% of S elements, with O/C of 0.65 and C/S of 14.6 (Ho et al., 2015).

In the case of BC/Fuc_75, the XPS confirmed the chemistry of the membrane with a surface composition dominated by 67.6% of carbon and 31.7% of oxygen with a small amount of sulphur (0.7%), which translates into O/C and C/S atomic ratios of 0.47 and 96.6, respectively (Table 2). The low relative abundance of S element is related with the fact that the BC/Fuc_75 membrane is composed of two polysaccharides, namely 57 wt.% of BC and 43 wt.% of fucoidan (Table 1), whose main polymeric chains are primarily composed of carbon and oxygen. Overall, these results provide further confirmation of the inclusion of the algal sulphated polysaccharide within the three-dimensional network of the bacterial exopolysaccharide.

Table 2 XPS data for pure BC, fucoidan and BC/Fuc membranes.

Samples	Atomic composition / % [a]			O/C	C/S
	C	O	S		
BC	62.4	37.6	–	0.60	–
Fuc	60.2	35.7	4.1	0.59	14.7

BC/Fuc_75	67.6	31.7	0.7	0.47	96.6

The C1s high-resolution spectra (Fig. 4B) of the pure BC and fucoidan samples can be deconvoluted into three components, namely a major peak at 286.6 eV (53.0% for BC and 65.4% for Fuc) allocated to the C–O and C–OH bonds, a distinguished peak at 285.0 eV (27.6% for BC and 19.0% for Fuc) assigned to the C–C and C–H bonds and the third one at 288.1 eV (19.4% for BC and 15.6% for Fuc) ascribed to the O–C–O and C=O bonds (Ho et al., 2015; Li et al., 2009). These C1s photoemission peaks correspond to signature bonds of polysaccharides in general.

Regarding the BC/Fuc_75 membrane, four C1s peaks were identified at around 285.0 eV (63.2%), 286.8 eV (28.6%) and 288.6 eV (8.2%) corresponding to C–H and C–C, C–OH/C–O and O–C–O/C=O bonds, respectively, as epitomized in Fig. 4B. Here, the percentage of each peak is different when compared with the individual compounds with a strong increase in the contribution of the C–C component (285.0 eV).

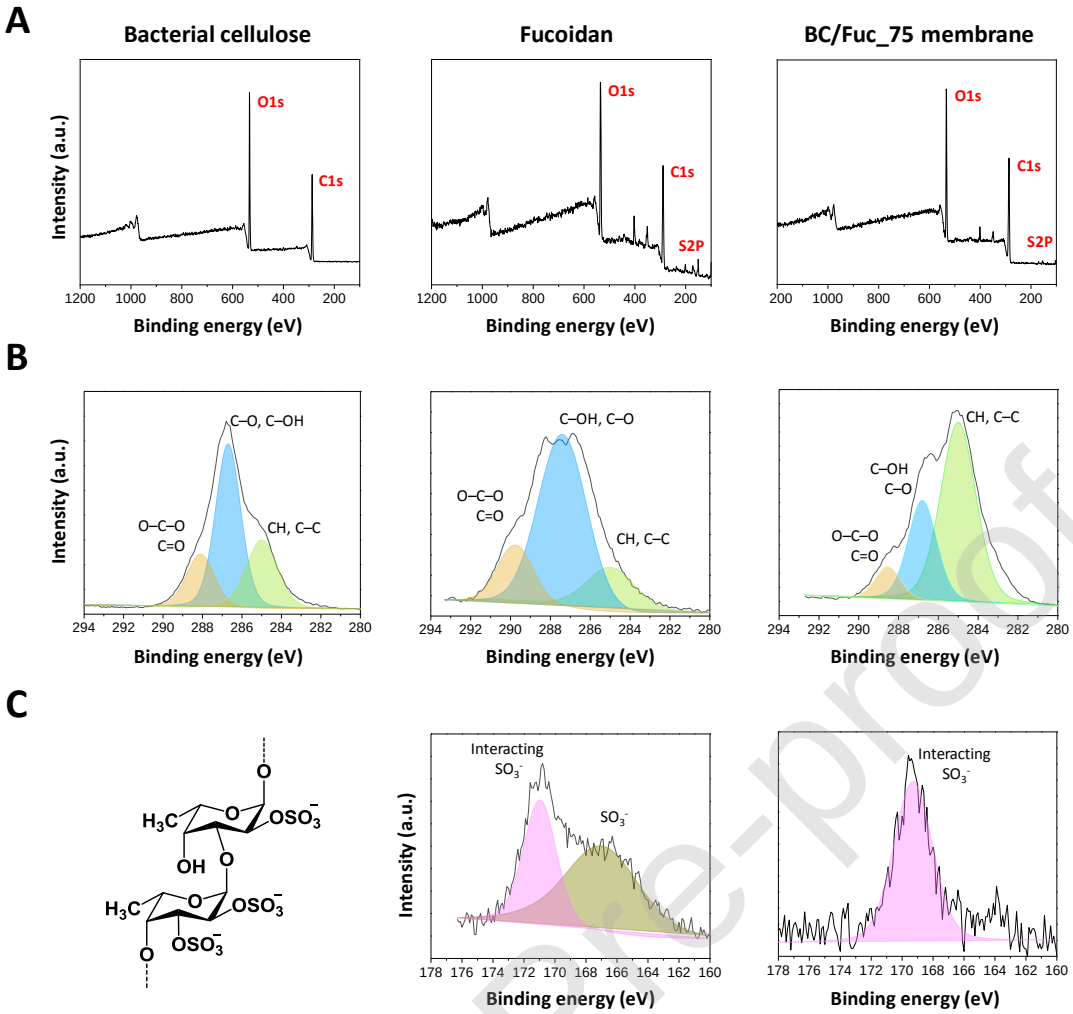

Fig. 4. (A) XPS survey spectra of pure BC, fucoidan and BC/Fuc_75, (B) XPS high-resolution C1s spectra of pure BC, fucoidan and BC/Fuc_75, and (C) fucoidan structure, XPS high-resolution S2p spectra of fucoidan and BC/Fuc_75 membrane.

The deconvolution of the S2p spectral peak of fucoidan (Fig. 4C) puts in evidence two chemical environments of sulphur with photoemission at *ca*. 167.0 eV (61.4%) and 170.9 eV (38.6%) corresponding to the hexavalent sulphur bound to oxygen, namely the $-OSO_3^-$ and interacting $-OSO_3^-$ group, respectively (Romanchenko, Levdansky, Levdansky, & Kuznetsov, 2015). For the BC/Fuc_75 membrane only one sulphur environment was visible at a binding energy of 169.3 eV (100%) corresponding to the interacting $-OSO_3^-$ group. This is a clear indication of the presence of interactions of

the fucoidan sulfonate group with other components that alter the environment of these moieties (Ho et al., 2015).

3.2. Microstructure

The morphology and topography of the pure BC and BC/Fuc membranes were assessed by HR-FESEM and 3D confocal profilometry, as depicted in Fig. 5 and Fig. 6, respectively. A close look at the surface and cross-section micrographs of the pure BC membrane (Fig. 5A) shows its characteristic morphological features, namely the nanofibrillar and lamellar microstructure (Klemm et al., 2018). Regarding the BC/Fuc membranes (Fig. 5B,C), a notable change in the surface and cross-sectional morphology was observed upon incorporation of the sulphated polysaccharide that concealed the nanofibrils and filled the lamellar spaces of the BC porous network. This is mostly evident in the case of BC/Fuc_75 that contains a superior content of fucoidan (573±15 mg of fucoidan per cm^3 of membrane, Table 1).

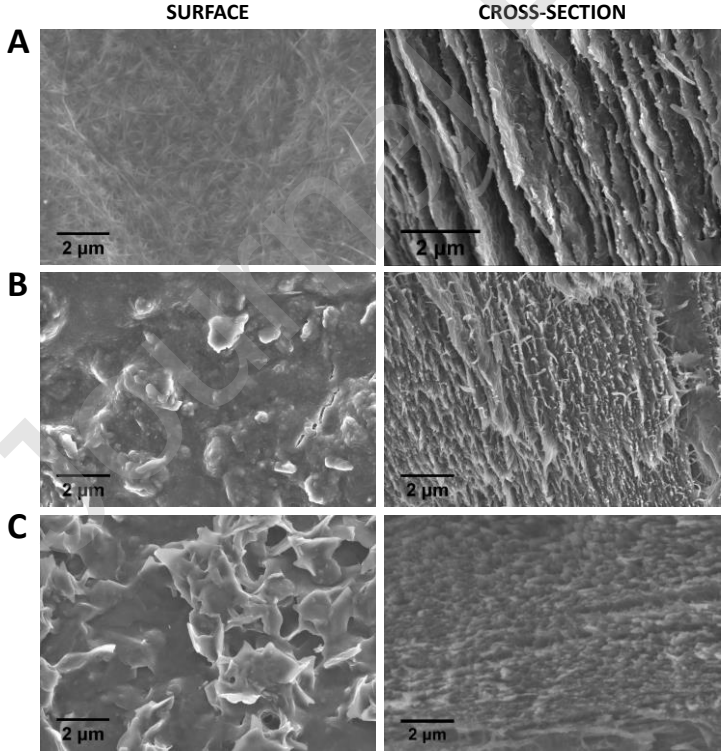

Fig. 5. HR-FESEM micrographs of the surface (left) and cross-section (right) of (A) BC, (B) BC/Fuc_50 and (C) BC/Fuc_75 membranes with a magnification of ×10.0k.

The surfaces of the membranes were further analysed by a 3D optical profilometer to investigate the areal surface texture. The data displayed in Fig. 6 demonstrate the different surface topographies of the three membranes at the macroscale, with the BC/Fuc membranes (Fig. 6B,C) exhibiting more "peaks" and "valleys" than the pure BC membrane (Fig. 6A). Furthermore, the height-descriptive 3D parameters point to the presence of surface microroughness with S_a (arithmetical mean height of the surface; ISO 25178) values of *ca*. 2 µm for BC, 5 µm for BC/Fuc_50 and 18 µm for BC/Fuc_75. The increasing microroughness with the increasing content of fucoidan agrees with the HR-FESEM micrographs of the membranes surface (Fig. 5), where the surface irregularities are higher for the membrane with the biggest fucoidan content (573±15 mg of fucoidan per cm^3 of membrane, Table 1).

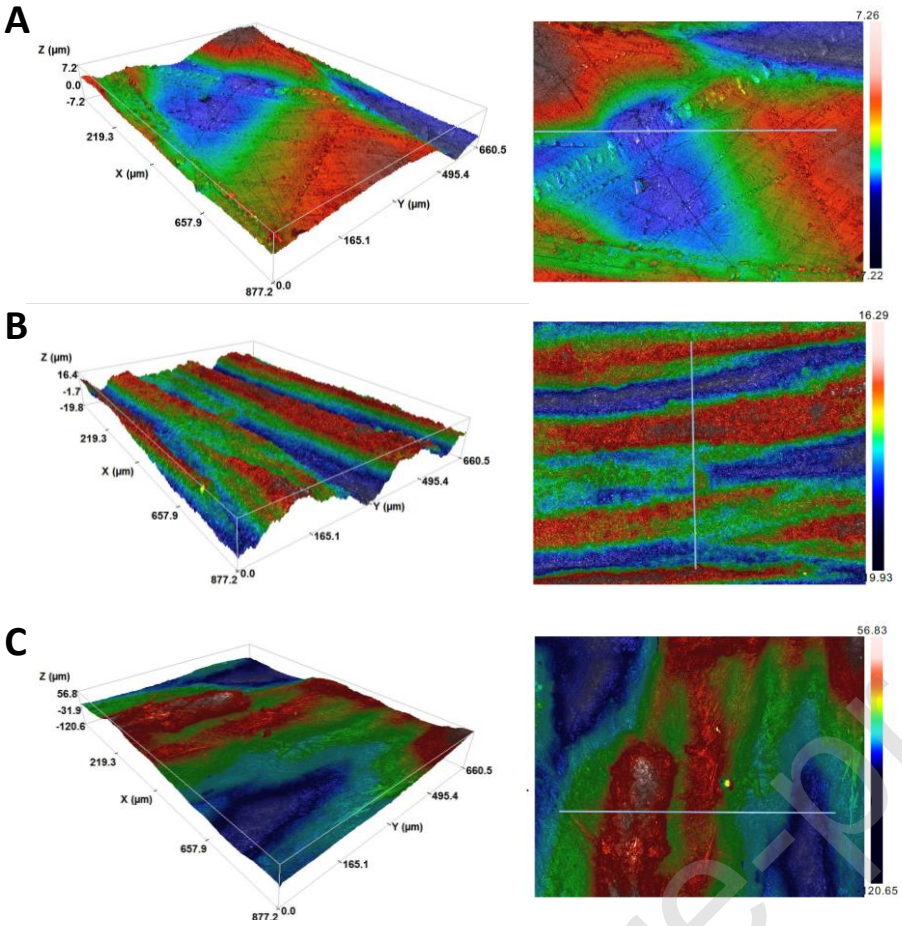

Fig. 6. Surface 3D (left) and 2D (right) mapping plots of (A) pure BC, (B) BC/Fuc_50 and (C) BC/Fuc_75 membranes with a 20× magnification; darker colours correspond with deeper surfaces.

3.3. Thermal-oxidative stability and dynamic mechanical properties

The thermal-oxidative stability and degradation profiles of the BC/Fuc membranes (and the corresponding pure components) were studied under nitrogen and oxygen atmospheres, as displayed in Fig. 7A and B, respectively. Under the inert nitrogen atmosphere, BC presents a single weight-loss profile with maximum decomposition temperature of 342 °C that is ascribed to the cellulose skeleton pyrolysis (Wang, Liu, Luo, Wen, & Cen, 2007), and a total residue of *ca*. 20% at 800 °C in accordance with data published elsewhere (Vilela, Moreirinha, Almeida, Silvestre, & Freire, 2019). On

the other hand, fucoidan exhibits, apart from the initial dehydration (25–179 °C, loss of *ca*. 15%), two weight-loss degradation pathway with maximum decomposition temperatures of 232 °C (loss of *ca*. 26%) and 691 °C (loss of *ca*. 59.5%) and a final residue of *ca*. 28%. The moisture content of this sulphated polysaccharide agrees with the values reported in previous studies for fucoidan extracted from *F. vesiculosus* (Anastasakis, Ross, & Jones, 2011; Rodriguez-Jasso et al., 2011). Furthermore, the two weight-loss steps are major and minor devolatilization processes as claimed by Monsur and co-workers for fucoidan extracted from *Turbinaria turbinate* (Monsur, Jaswir, Simsek, Amid, & Alam, 2017), which correspond to the breakdown of glycosidic bonds and conversion into ash, respectively, as described for fucoidan extracted from *Saccharina japonica* (Saravana, Cho, Woo, & Chun, 2018). In relation with the BC/Fuc membranes, the TGA tracing evidences the singular features of each of the individual components, *viz*. BC and fucoidan, with thermal stability up to 180–200 °C and a final residue of *ca*. 29% for BC/Fuc_50 and 32% for BC/Fuc_75 at 800 °C (Fig. 7A).

Hinted at the possibility of using these BC/Fuc membranes as proton-exchange membranes in PEFCs, which operate under an oxygen-containing atmosphere, their TGA profiles were also assessed under an oxidative oxygen atmosphere (Fig. 7B). Herein, BC exhibits a two-step weight-loss degradation profile with maximum decomposition temperatures of 342 °C (loss of *ca*. 45%) and 431 °C (loss of *ca*. 89%) and reaches total degradation with no final residue (Vilela, Gadim, Silvestre, Freire, & Figueiredo, 2016; Vilela et al., 2017). Regarding fucoidan, a three-step weight-loss degradation profile was observed with maximum decomposition temperatures of 234 °C (loss of *ca*. 26%), 449 °C (loss of *ca*. 63%) and 726 °C (loss of *ca*. 75%) with a final residue *ca*. 24%. The thermal stability profiles of fucoidan under inert (Fig. 7A) and oxidative (Fig. 7B) atmospheres are comparable, particularly in the total residue content

at 800 °C. A similar behaviour was also reported by Anastasakis and co-workers for fucoidan extracted from *F. vesiculosus*, which was associated with the sulphate groups and the presence of different metals (*e.g.*, Ca, Fe, K, Mg, Na and Sr) (Anastasakis et al., 2011).

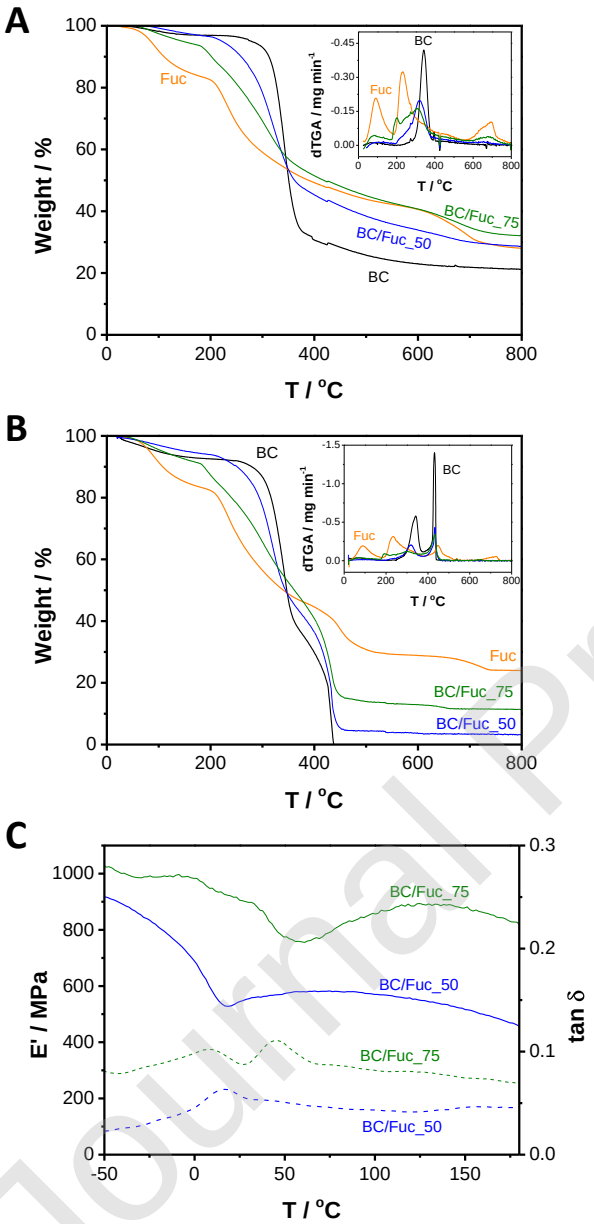

Fig. 7. Thermograms of pure BC, fucoidan and membranes BC/Fuc_50 and BC/Fuc_75 under (A) N_2 and (B) O_2 atmospheres, with the inset curves representing the corresponding derivatives; (C) storage modulus (*E*', — solid lines) and loss-factor (tan *δ*, --- dashed lines) curves of BC/Fuc_50 and BC/Fuc_75 membranes.

In the case of the BC/Fuc membranes, the TGA profile under oxidative atmosphere reflects the combination between the two individual components and the attained weight-losses confirmed their oxidative stability up to 180–200 °C with a final residue of *ca*. 4% for BC/Fuc_50 and 11% for BC/Fuc_75 at 800 °C (Fig. 7B).

Comparing these membranes with Nafion™ (*i.e*., the commercial proton-exchange membrane used in PEFCs), it is clear that their thermal stability is lower than the *ca*. 290 °C of the benchmark ionomer (Gadim et al., 2016). Nevertheless, these results unveil the good thermal-oxidative stability of the BC/Fuc membranes up to temperatures in the range of 180–200 °C, which is a solid evidence that these nanomaterials will be thermally stable under the standard operating temperature of PEFCs, < 100 °C.

The dynamic mechanical performance of the BC/Fuc membranes was studied by DMA and the tensile storage modulus (E') and loss-factor (tan δ) data are illustrated in Fig. 7C. The inaptitude of the fucoidan to form a film or membrane hindered its analysis and thus no figures are reported. In the case of the pure BC, it is described in literature that there is practically no variation of the *E*' values with temperature except for the slight change between –10 °C and 40 °C, which is normally ascribed to the plasticizing effect of water (Gadim et al., 2014; Lacerda, Barros-Timmons, Freire, Silvestre, & Neto, 2013).

Concerning the BC/Fuc membranes, Fig. 7C shows that the BC/Fuc_75 has better dynamic mechanical properties than BC/Fuc_50 for the full range of temperatures from –50 °C to 180 °C. In the case of the BC/Fuc_50 membrane, the *E*' drops from 918 MPa at –50 °C to 527 MPa at 18.5 °C, then increases to 582 MPa at 75 °C and drops to 460 MPa at 180 °C. This storage modulus curve is matched by the loss-factor data with a

peak in the range of –0.5 °C to 30 °C, which might be related with the plasticizing effect of water, given that this membrane contains approximately 1% of water, as determined by TGA (Fig. 7A). For the BC/Fuc_75 membrane, the *E*' varies between 1033 MPa at –50 °C to 813 MPa at 180 °C with the minimum value of 755 MPa at 61 °C. This profile is paired with two tan δ peaks with maximum loss-factor values at 8.3 °C and 44.5 °C, the former probably also linked with the plasticizing effect of water (*ca*. 3% of water determined by TGA, Fig. 7A) and the latter to the fucoidan fraction. These natural-based membranes exhibit storage modulus values that are lower than, for example, the membranes composed of BC and poly(4-styrene sulfonic acid) (PSSA), which is a synthetic polyelectrolyte that also contains sulfonic acid groups (Gadim et al., 2014). Albeit the inferior *E*' values obtained for BC/Fuc_50, both membranes kept reasonable mechanical integrity and have a better dynamic mechanical performance than the corresponding commercial proton-exchange membrane used in PEFCs, *viz*. Nafion™, whose storage modulus decreases from about 174 MPa at –30 °C to 385 kPa at 180 °C (Gadim et al., 2016).

3.4. Moisture-uptake capacity

BC and fucoidan are both hydrophilic materials with the aptitude to absorb environmental humidity. Therefore, the moisture-uptake capacity of both BC/Fuc_50 and BC/Fuc_75 membranes were measured to evaluate their ability to absorb moisture that strongly affects the protonic conductivity (Bose et al., 2011). Hence, the BC/Fuc membranes, the pure BC membrane and the fucoidan powder were placed in a chamber with controlled humidity, namely 98% RH, at room temperature for 48 h. According to Fig. 8A, all samples absorbed moisture during that period of time with the pure BC membrane and fucoidan powder exhibiting the lowest (22±2%) and highest (68±3%)

values, respectively. The moisture-uptake capacity obtained for BC is comparable to recently published data (Vilela, Moreirinha, Domingues, et al., 2019). In the case of the BC/Fuc membranes, the BC/Fuc_75 (with 57 wt.% of BC and 43 wt.% of fucoidan) absorbed more environmental humidity (45±3%) than the BC/Fuc_50 (32±2%), which is composed of 67 wt.% of BC and 33 wt.% of fucoidan. This was expectable given the highly hygroscopic nature of the algae sulphated polysaccharide (Luthuli et al., 2019).

Furthermore, it is worth mentioning that these BC/Fuc membranes present a moisture-uptake capacity that is similar or even higher than the water absorption of the commercial Nafion™ (around 38%) when soaked in water at 100 °C for 1 h (DuPont™, 2016). These results, together with the good wet-dimensional stability of BC, point to nanomaterials that will exhibit protonic conductivity since proton transport is closely associated to the aqueous domains formed within the structure of the membranes (Vilela, Silvestre, et al., 2019), as will be discussed in the following paragraphs.

3.5. Protonic conductivity measurements

The proton conducting behaviour of the BC/Fuc natural-based membranes was investigated by EIS in a through-plane configuration. Starting with the pure BC membrane (thickness: 35±1 μm), Fig. 8B shows that the bacterial exopolysaccharide is a poor ionic conductor, as already reported in other studies (Gadim et al., 2014, 2017), with conductivity (σ) values ranging from 1.7×10^{-7} mS cm^{-1} at 40 °C and 40% RH to 6.3×10^{-2} mS cm^{-1} at 94 °C and 98% RH. As expected, the protonic conductivity increases with increasing relative humidity (40–98% RH) and temperature (40–94 °C). However, and since the proton motion is deeply correlated with humidification, the RH is the parameter that mostly influences the protonic conductivity (Vilela, Silvestre, et al., 2019), where an augment of the RH from 40% to 98% (at 60 °C) increased the

conductivity by five orders of magnitude from 1.8×10^{-7} mS cm^{-1} to 2.6×10^{-2} mS cm^{-1}. When temperature is involved, the effect on the conductivity is less pronounced with a maximum increase of two orders of magnitude from 5.4×10^{-7} mS cm^{-1} at 40 °C to 1.2×10^{-5} mS cm^{-1} at 94 °C (at 60% RH, Fig. 8B).

The comparison of these values with the protonic conductivity data obtained for the other two nanoscale forms of cellulose, *viz*. cellulose nanofibrils (CNFs) and cellulose nanocrystals (CNCs), shows that the BC membrane with no ionic functionalization (with only hydroxyl groups) presents a protonic conductivity (0.063 mS cm^{-1} at 94 °C and 98% RH, thickness: 35±1 μm) that is similar to CNFs (0.05 mS cm^{-1} at 100 °C and nominal 100% RH, thickness: 32 μm) but much lower than the CNCs (2.5 mS cm^{-1} at 90 °C and nominal 100% RH, thickness: 30 μm) (Bayer et al., 2016). Although the presence of sulfonic acid groups enhances the conductivity of CNCs, it is also likely to compromise their thermal and mechanical stability in comparison to CNFs (as noted by Bayer and co-workers (Bayer et al., 2016)) and to BC. Therefore, the resistance and mechanical stability of BC when exposed to high humidity and temperature are key advantages in the context of PEFCs operation since the proton-exchange membrane is subjected to highly variable humidity conditions and highly oxidative environment imposed by the catalyst.

The polyelectrolytic nature of fucoidan was confirmed by the Arrhenius-type plots of the BC/Fuc_50 (thickness: 52±5 μm) and BC/Fuc_75 (thickness: 79±6 μm) membranes displayed in Fig. 8C and Fig. 8D, respectively. Here, the behaviour is the same as for BC, where the protonic conductivity increases with RH and temperature, but the values are higher than those obtained for the pure exopolysaccharide. In fact, the incorporation of fucoidan into the porous BC network led to a maximum increase of two and three orders of magnitude in the protonic conductivity, from 3.7×10^{-4} mS cm^{-1}

for pure BC to 7.7×10^{-2} mS cm^{-1} for BC/Fuc_50 and 1.3×10^{-1} mS cm^{-1} for BC/Fuc_75 at 80% RH and 94 °C. It is evident that BC/Fuc_50 (33 wt.% of fucoidan) presents lower conductivity values than BC/Fuc_75 (43 wt.% of fucoidan) for 40 and 60% RH, but this difference dissipates for higher RH values, namely 80 and 98%. For instance, the conductivities of BC/Fuc_50 and BC/Fuc_75 are 6.5×10^{-6} mS cm^{-1} and 1.8×10^{-5} mS cm^{-1} at 40% RH (and 80 °C), while at 98% RH (and 80 °C) the conductivity of BC/Fuc_50 is 7.6×10^{-1} mS cm^{-1} and of BC/Fuc_75 is 7.8×10^{-1} mS cm^{-1}.

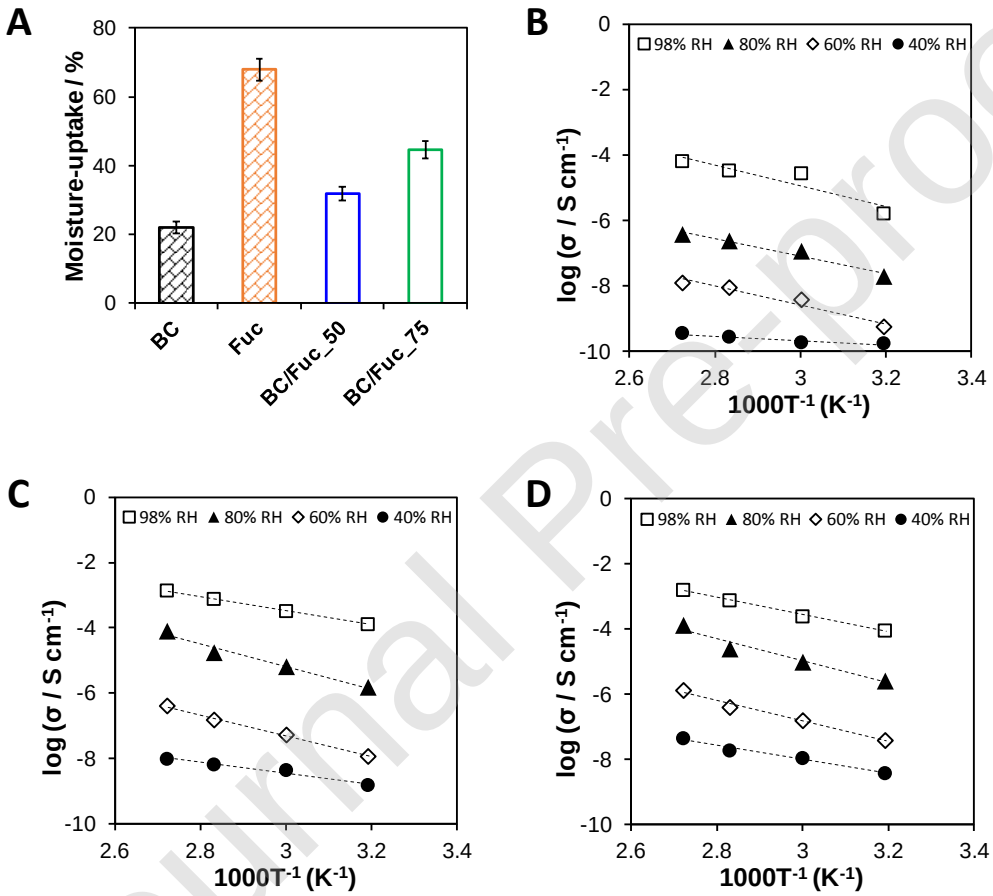

Fig. 8. (A) Moisture-uptake capacity of BC, fucoidan, BC/Fuc_50 and BC/Fuc_75 after 48 h at RT and 98% RH, and (B–D) Arrhenius-type plots of the through-plane protonic conductivity (σ) of (B) BC, (C) BC/Fuc_50 and (D) BC/Fuc_75 membranes at different RH (40, 60, 80 and 98%), the (---) dashed lines are linear fits to the Arrhenius model.

The maximum protonic conductivity was reached for BC/Fuc_75 membrane with 1.6 mS cm^{-1} at 98% RH and 94 °C (Fig. 8D), which is higher than the maximum value obtained for example by the ion-conducting membrane composed of BC and triethanolamine (1 mol dm^{-3}) that reached 0.7 mS cm^{-1} at 80 °C, also measured in the trough-plane configuration (De Salvi et al., 2014). Nevertheless, this maximum conductivity obtained for BC/Fuc_75 is two orders of magnitude inferior to that of poly(4-styrene sulfonic acid)/BC nanocomposite membranes ($\sigma_{max} \approx 100$ mS cm^{-1} at 98% RH and 94 °C, under similar operating conditions) that also contain sulfonic acid groups (Gadim et al., 2014). Furthermore, the conductivity of the BC/Fuc membranes is also two orders of magnitude lower than the benchmark Nafion™ (Cele & Ray, 2009; Rosero-Navarro, Domingues, Sousa, Ferreira, & Figueiredo, 2014b). Still, the mass ratio of fucoidan in the membranes (BC:Fuc is 2:1 for BC/Fuc_50 and 4:3 for BC/Fuc_75) can be tuned to higher values to control their proton conducting behaviour and thus obtain superior protonic conductivity.

The protonic conductivity dependence on temperature was also validated by the fact that the data follows the linear Arrhenius-type behaviour: $\sigma = \sigma_0 e^{-E_a(RT)^{-1}}$, where σ_0 is a pre-exponential term, E_a is the activation energy for ion transport, R is the gas constant, and T is the absolute temperature (Gadim et al., 2014; Petrowsky & Frech, 2009). The estimated activation energies for proton transport varied from 16–63 kJ mol^{-1} for BC, 32–69 kJ mol^{-1} for BC/Fuc_50 and 54–74 kJ mol^{-1} for BC/Fuc_75, which are higher than the values typically reported for Nafion™ (E_a = 13−32 kJ mol^{-1}) (Rosero-Navarro, Domingues, Sousa, Ferreira, & Figueiredo, 2014a; Rosero-Navarro et al., 2014b). In the case of BC/Fuc_75, it seems that the E_a decreased with increasing RH but that tendency is not clearly visible for the BC/Fuc_50 membrane.

From the similar E_a values of BC and the two BC/Fuc membranes, it is possible to withdraw information about the conduction mechanisms involved in proton transport, as discussed elsewhere (Eikerling, Kornyshev, Kuznetsov, Ulstrup, & Walbran, 2001; Miyake & Rolandi, 2016). In fact, the pure BC and both BC/Fuc membranes are most likely dominated by the same conduction mechanism(s), where some of the values are within the range consistent with the Grotthuss-like water-mediated mechanism, *viz*. 10–50 kJ mol^{-1} (Grancha et al., 2016), and the vehicle mechanism, *viz*. 50–90 kJ mol^{-1} (Bayer et al., 2016). The first case is dominated by the hopping of protons between neighbouring and hydrogen-bonded water molecules (Miyake & Rolandi, 2016), whereas the second is characterized by proton diffusion with water where the ions are transported by a vehicle such as the hydronium ion (H_3O^+) (Kreuer, 1996).

Given these results, the combination between the hydrocolloid exopolysaccharide BC and the algae sulphated polysaccharide fucoidan was enough to develop fully-biobased membranes with moderate protonic conductivity. The catalogue of properties of these water-mediated proton conductor membranes, namely good thermal-oxidative stability, dynamic mechanical performance, moisture-uptake capacity and protonic conductivity, reflect their potential application as a proton-exchange membrane, which is one of the key components of PEFCs (Vilela, Silvestre, et al., 2019).

4. Conclusions

BC, a hydrocolloid polysaccharide gel produced by non-pathogenic bacteria, and fucoidan, a bioactive water-soluble polysaccharide derived from brown algae, were used to design fully bio-based conductive natural-based separators for application in polymer electrolyte fuel cells. The collected data confirm that the proton-exchange membranes have a good thermal-oxidative stability up to almost 200 °C in both N_2 and O_2

atmospheres, and good dynamic mechanical performance with a minimum storage modulus of *ca*. 460 MPa. Furthermore, the brownish BC/Fuc-based membranes display a linear behaviour in the traditional Arrhenius-type plots with a maximum protonic conductivity of 1.6 mS cm^{-1} at 94 °C and 98% RH (through-plane configuration) that is strongly related to humidification. Hence, the results hint at the possibility of using these conductive and fully bio-based membranes as environmentally friendly alternatives to other proton-exchange membranes for application in PEFCs.

Acknowledgements

This work was developed within the scope of the project CICECO – Aveiro Institute of Materials (FCT Ref. UID/CTM/50011/2019) and TEMA (FCT Ref. UID/EMS/00481/2019 and CENTRO-01-0145-FEDER-022083), financed by national funds through the FCT/MEC. The research contract of C.V. is funded by national funds (OE), through FCT – Fundação para a Ciência e a Tecnologia, I.P., in the scope of the framework contract foreseen in the numbers 4, 5 and 6 of article 23, of the Decree-Law 57/2016, of August 29, changed by Law 57/2017, of July 19. The research contracts of E.M.D. and S.A.O.S. are funded by projects UniRCell (SAICTPAC/0032/2015, POCI-01-0145-FEDER-016422) and AgroForWealth (CENTRO-01-0145-FEDER-000001), respectively. FCT is also acknowledge for the doctoral grant to A.C.Q.S. (SFRH/BD/140230/2018) and research contracts under Stimulus of Scientific Employment 2017 to G.G. (CEECIND/01913/2017) and C.S.R.F. (CEECIND/00464/2017). The authors also wish to thank ALGAplus (Produção e comércio de algas e seus derivados, Lda, Portugal) for kindly providing the seaweed samples and Dr. Filipe J. Oliveira (DeMac, University of Aveiro) for the help with the non-contact 3D optical profilometer.

References

Ale, M. T., & Meyer, A. S. (2013). Fucoidans from brown seaweeds: an update on structures, extraction techniques and use of enzymes as tools for structural elucidation. *RSC Advances*, *3*(22), 8131–8141. https://doi.org/10.1039/C3RA23373A

Anastasakis, K., Ross, A. B., & Jones, J. M. (2011). Pyrolysis behaviour of the main carbohydrates of brown macro-algae. *Fuel*, *90*(2), 598–607. https://doi.org/10.1016/J.FUEL.2010.09.023

Aver'yanova, I. O., Bogomolov, D. Y., & Poroshin, V. V. (2017). ISO 25178 standard for three-dimensional parametric assessment of surface texture. *Russian Engineering Research*, *37*(6), 513–516. https://doi.org/10.3103/S1068798X17060053

Bayer, T., Cunning, B. V., Selyanchyn, R., Nishihara, M., Fujikawa, S., Sasaki, K., & Lyth, S. M. (2016). High temperature proton conduction in nanocellulose membranes: Paper fuel cells. *Chemistry of Materials*, *28*(13), 4805–4814. https://doi.org/10.1021/acs.chemmater.6b01990

Bellamy, L. J. (1975). *The infrared spectra of complex molecules* (3rd ed.). London, UK: Chapman and Hall, Ltd.

Bose, S., Kuila, T., Nguyen, T. X. H., Kim, N. H., Lau, K., & Lee, J. H. (2011). Polymer membranes for high temperature proton exchange membrane fuel cell: Recent advances and challenges. *Progress in Polymer Science*, *36*(6), 813–843. https://doi.org/10.1016/J.PROGPOLYMSCI.2011.01.003

Catarino, M. D., Silva, A. M. S., & Cardoso, S. M. (2018). Phycochemical constituents and biological activities of Fucus spp. *Marine Drugs*, *16*(8), 249.

https://doi.org/10.3390/md16080249

Cele, N., & Ray, S. S. (2009). Recent progress on Nafion-based nanocomposite membranes for fuel cell applications. *Macromolecular Materials and Engineering*, *294*(11), 719–738. https://doi.org/10.1002/mame.200900143

Chen, S., & Huang, Y. (2015). Bacterial cellulose nanofibers decorated with phthalocyanine: Preparation, characterization and dye removal performance. *Materials Letters*, *142*, 235–237. https://doi.org/10.1016/J.MATLET.2014.12.036

Chen, W., Li, N., Ma, Y., Minus, M. L., Benson, K., Lu, X., Wang, X., Ling, X., & Zhu, H. (2019). Super strong and tough hydrogel through physical crosslinking and molecular alignment. *Biomacromolecules*. https://doi.org/10.1021/acs.biomac.9b01223

De Salvi, D. T. B., Barud, H. S., Pawlicka, A., Mattos, R. I., Raphael, E., Messaddeq, Y., & Ribeiro, S. J. L. (2014). Bacterial cellulose/triethanolamine based ion-conducting membranes. *Cellulose*, *21*(3), 1975–1985. https://doi.org/10.1007/s10570-014-0212-8

DuPont™. (2016). Nafion® N115, N117, N1110 - Ion exchange materials, Product Bulletin P-12. Retrieved September 24, 2019, from https://www.chemours.com/Nafion/en_US/assets/downloads/nafion-extrusion-cast-membranes-product-information.pdf

Eikerling, M., Kornyshev, A. A., Kuznetsov, A. M., Ulstrup, J., & Walbran, S. (2001). Mechanisms of proton conductance in polymer electrolyte membranes. *Journal of Physical Chemistry B*, *105*(17), 3646–3662. https://doi.org/10.1021/jp003182s

Erel-Unal, I., & Sukhishvili, S. A. (2008). Hydrogen-bonded multilayers of a neutral polymer and a polyphenol. *Macromolecules*, *41*(11), 3962–3970. https://doi.org/10.1021/ma800186q

Espinosa-Velázquez, G., Ramos-de-la-Peña, A. M., Montanez, J., & Contreras-Esquivel, J. C. (2018). Rapid physicochemical characterization of innovative fucoidan/fructan powders by ATR–FTIR. *Food Science and Biotechnology*, *27*(2), 411–415. https://doi.org/10.1007/s10068-017-0265-1

Fan, H., Wang, L., Feng, X., Bu, Y., Wu, D., & Jin, Z. (2017). Supramolecular hydrogel formation based on tannic acid. *Macromolecules*, *50*(2), 666–676. https://doi.org/10.1021/acs.macromol.6b02106

Foresti, M. L., Vázquez, A., & Boury, B. (2017). Applications of bacterial cellulose as precursor of carbon and composites with metal oxide, metal sulfide and metal nanoparticles: A review of recent advances. *Carbohydrate Polymers*, *157*, 447–467. https://doi.org/10.1016/J.CARBPOL.2016.09.008

Foster, E. J., Moon, R. J., Agarwal, U. P., Bortner, M. J., Bras, J., Camarero-Espinosa, S., Chan, K. J., Clift, M. J. D., Cranston, E. D., Eichhorn, S. J., Fox, D. M., Hamad, W. Y., Heux, L., Jean, B., Korey, M., Nieh, W., Ong, K. J., Reid, M. S., Renneckar, S., Roberts, R., Shatkin, J. A., Simonsen, J., Stinson-Bagby, K., Wanasekara, N., & Youngblood, J. (2018). Current characterization methods for cellulose nanomaterials. *Chemical Society Reviews*, *47*(8), 2609–2679. https://doi.org/10.1039/c6cs00895j

Gadim, T. D. O., Figueiredo, A. G. P. R., Rosero-Navarro, N. C., Vilela, C., Gamelas, J. A. F., Barros-Timmons, A., Neto, C. P., Silvestre, A. J. D., Freire, C. S. R., & Figueiredo, F. M. L. (2014). Nanostructured bacterial cellulose-poly(4-styrene sulfonic acid) composite membranes with high storage modulus and protonic conductivity. *ACS Applied Materials & Interfaces*, *6*(10), 7864–7875. https://doi.org/10.1021/am501191t

Gadim, T. D. O., Loureiro, F. J. A., Vilela, C., Rosero-Navarro, N., Silvestre, A. J. D.,

Freire, C. S. R., & Figueiredo, F. M. L. (2017). Protonic conductivity and fuel cell tests of nanocomposite membranes based on bacterial cellulose. *Electrochimica Acta*, *233*, 52–61. https://doi.org/10.1016/j.electacta.2017.02.145

Gadim, T. D. O., Vilela, C., Loureiro, F. J. A., Silvestre, A. J. D., Freire, C. S. R., & Figueiredo, F. M. L. (2016). Nafion® and nanocellulose: a partnership for greener polymer electrolyte membranes. *Industrial Crops and Products*, *93*, 212–218. https://doi.org/10.1016/j.indcrop.2016.01.028

Grancha, T., Ferrando-Soria, J., Cano, J., Amorós, P., Seoane, B., Gascon, J., Bazaga-García, M., Losilla, E. R., Cabeza, A., Armentano, D., & Pardo, E. (2016). Insights into the dynamics of Grotthuss mechanism in a proton-conducting chiral bioMOF. *Chemistry of Materials*, *28*(13), 4608–4615. https://doi.org/10.1021/acs.chemmater.6b01286

Greenspan, L. (1977). Humidity fixed points of binary saturated aqueous solutions. *Journal of Research of the National Bureau of Standards A Physics and Chemistry*, *81*(1), 89–96. https://doi.org/10.6028/jres.081A.011

Ho, T. T. M., Bremmell, K. E., Krasowska, M., Stringer, D. N., Thierry, B., & Beattie, D. A. (2015). Tuning polyelectrolyte multilayer structure by exploiting natural variation in fucoidan chemistry. *Soft Matter*, *11*(11), 2110–2124. https://doi.org/10.1039/C4SM02552K

Jiang, Gao-peng, Zhang, J., Qiao, J., Jiang, Y., Zarrin, H., Chen, Z., & Hong, F. (2015). Bacterial nanocellulose/Nafion composite membranes for low temperature polymer electrolyte fuel cells. *Journal of Power Sources*, *273*, 697–706. https://doi.org/10.1016/j.jpowsour.2014.09.145

Jiang, Gaopeng, Qiao, J., & Hong, F. (2012). Application of phosphoric acid and phytic acid-doped bacterial cellulose as novel proton-conducting membranes to PEMFC.

International Journal of Hydrogen Energy, *37*(11), 9182–9192. https://doi.org/10.1016/j.ijhydene.2012.02.195

Klemm, D., Cranston, E. D., Fischer, D., Gama, M., Kedzior, S. A., Kralisch, D., Kramer, F., Kondo, T., Lindström, T., Nietzsche, S., Petzold-Welcke, K., & Rauchfuß, F. (2018). Nanocellulose as a natural source for groundbreaking applications in materials science: Today's state. *Materials Today*, *21*(7), 720–748. https://doi.org/10.1016/j.mattod.2018.02.001

Kreuer, K. D. (1996). Proton conductivity: Materials and applications. *Chemistry of Materials*, *8*(3), 610–641. https://doi.org/10.1021/cm950192a

Lacerda, P. S. S., Barros-Timmons, A. M. M. V, Freire, C. S. R., Silvestre, A. J. D., & Neto, C. P. (2013). Nanostructured composites obtained by ATRP sleeving of bacterial cellulose nanofibers with acrylate polymers. *Biomacromolecules*, *14*, 2063–2073. https://doi.org/10.1021/bm400432b

Lee, E. J., & Lim, K.-H. (2014). Polyelectrolyte complexes of chitosan self-assembled with fucoidan: An optimum condition to prepare their nanoparticles and their characteristics. *Korean Journal of Chemical Engineering*, *31*(4), 664–675. https://doi.org/10.1007/s11814-013-0243-0

Li, J., Wan, Y., Li, L., Liang, H., & Wang, J. (2009). Preparation and characterization of 2,3-dialdehyde bacterial cellulose for potential biodegradable tissue engineering scaffolds. *Materials Science and Engineering: C*, *29*(5), 1635–1642. https://doi.org/10.1016/J.MSEC.2009.01.006

Luthuli, S., Wu, S., Cheng, Y., Zheng, X., Wu, M., & Tong, H. (2019). Therapeutic effects of fucoidan : A review on recent studies. *Marine Drugs*, *17*(9), 487. https://doi.org/10.3390/md17090487

Miyake, T., & Rolandi, M. (2016). Grotthuss mechanisms: from proton transport in

proton wires to bioprotonic devices. *Journal of Physics: Condensed Matter*, *28*, 023001. https://doi.org/10.1088/0953-8984/28/2/023001

Monsur, H. A., Jaswir, I., Simsek, S., Amid, A., & Alam, Z. (2017). Chemical structure of sulfated polysaccharides from brown seaweed (Turbinaria turbinata). *International Journal of Food Properties*, *20*(7), 1457–1469. https://doi.org/10.1080/10942912.2016.1211144

Nunes, S. C., Pereira, R. F. P., Sousa, N., Silva, M. M., Almeida, P., Figueiredo, F. M. L., & Bermudez, V. de Z. (2017). Eco-friendly red seaweed-derived electrolytes for electrochemical devices. *Advanced Sustainable Systems*, *1*(9), 1700070. https://doi.org/10.1002/adsu.201700070

Petrowsky, M., & Frech, R. (2009). Temperature dependence of ion transport: the compensated Arrhenius equation. *The Journal of Physical Chemistry B*, *113*(17), 5996–6000. https://doi.org/10.1021/jp810095g

Pielesz, A., & Biniaś, W. (2010). Cellulose acetate membrane electrophoresis and FTIR spectroscopy as methods of identifying a fucoidan in Fucus vesiculosus Linnaeus. *Carbohydrate Research*, *345*(18), 2676–2682. https://doi.org/10.1016/J.CARRES.2010.09.027

Rodriguez-Jasso, R. M., Mussatto, S. I., Pastrana, L., Aguilar, C. N., & Teixeira, J. A. (2011). Microwave-assisted extraction of sulfated polysaccharides (fucoidan) from brown seaweed. *Carbohydrate Polymers*, *86*(3), 1137–1144. https://doi.org/10.1016/J.CARBPOL.2011.06.006

Romanchenko, A. S., Levdansky, A. V., V. A. Levdansky, & B. N. Kuznetsov. (2015). Study of cellulose sulfates by X-ray photoelectron spectroscopy. *Russian Journal of Bioorganic Chemistry*, *41*(7), 719–724. https://doi.org/10.1134/S1068162015070134

Rosero-Navarro, N. C., Domingues, E. M., Sousa, N., Ferreira, P., & Figueiredo, F. M. (2014a). Protonic conductivity and viscoelastic behaviour of Nafion® membranes with periodic mesoporous organosilica fillers. *International Journal of Hydrogen Energy*, *39*(10), 5338–5349. https://doi.org/10.1016/j.ijhydene.2013.12.197

Rosero-Navarro, N. C., Domingues, E. M., Sousa, N., Ferreira, P., & Figueiredo, F. M. L. (2014b). Meso-structured organosilicas as fillers for Nafion® membranes. *Solid State Ionics*, *262*, 324–327. https://doi.org/10.1016/j.ssi.2013.09.058

Saravana, P. S., Cho, Y.-N., Woo, H.-C., & Chun, B.-S. (2018). Green and efficient extraction of polysaccharides from brown seaweed by adding deep eutectic solvent in subcritical water hydrolysis. *Journal of Cleaner Production*, *198*, 1474–1484. https://doi.org/10.1016/J.JCLEPRO.2018.07.151

Silva, N. H. C. S., Vilela, C., Marrucho, I. M., Freire, C. S. R., Pascoal Neto, C., & Silvestre, A. J. D. (2014). Protein-based materials: from sources to innovative sustainable materials for biomedical applications. *Journal of Materials Chemistry B*, *2*(24), 3715–3740. https://doi.org/10.1039/c4tb00168k

Silvestre, A. J. D., Freire, C. S. R., & Neto, C. P. (2014). Do bacterial cellulose membranes have potential in drug-delivery systems? *Expert Opinion on Drug Delivery*, *11*(7), 1113–1124. https://doi.org/10.1517/17425247.2014.920819

Thomas, B., Raj, M. C., B, A. K., H, R. M., Joy, J., Moores, A., Drisko, G. L., & Sanchez, C. (2018). Nanocellulose, a versatile green platform: from biosources to materials and their applications. *Chemical Reviews*, *118*(24), 11575–11625. https://doi.org/10.1021/acs.chemrev.7b00627

Torgbo, S., & Sukyai, P. (2018). Bacterial cellulose-based scaffold materials for bone tissue engineering. *Applied Materials Today*, *11*, 34–49. https://doi.org/10.1016/J.APMT.2018.01.004

Torres, F. G., Arroyo, J. J., & Troncoso, O. P. (2019). Bacterial cellulose nanocomposites: An all-nano type of material. *Materials Science and Engineering C*, *98*, 1277–1293. https://doi.org/10.1016/j.msec.2019.01.064

Trovatti, E., Serafim, L. S., Freire, C. S. R., Silvestre, A. J. D., & Neto, C. P. (2011). Gluconacetobacter sacchari: An efficient bacterial cellulose cell-factory. *Carbohydrate Polymers*, *86*(3), 1417–1420. https://doi.org/10.1016/j.carbpol.2011.06.046

Vilela, C., Gadim, T. D. O., Silvestre, A. J. D., Freire, C. S. R., & Figueiredo, F. M. L. (2016). Nanocellulose/poly(methacryloyloxyethyl phosphate) composites as proton separator materials. *Cellulose*, *23*(6), 3677–3689. https://doi.org/10.1007/s10570-016-1050-7

Vilela, C., Martins, A. P. C., Sousa, N., Silvestre, A. J. D., Figueiredo, F. M. L., & Freire, C. S. R. (2018). Poly(bis[2-(methacryloyloxy)ethyl] phosphate)/bacterial cellulose nanocomposites: Preparation, characterization and application as polymer electrolyte membranes. *Applied Sciences*, *8*(7), 1145. https://doi.org/10.3390/app8071145

Vilela, C., Moreirinha, C., Almeida, A., Silvestre, A. J. D., & Freire, C. S. R. (2019). Zwitterionic nanocellulose-based membranes for organic dye removal. *Materials*, *12*(9), 1404. https://doi.org/10.3390/ma12091404

Vilela, C., Moreirinha, C., Domingues, E. M., Figueiredo, F. M. L., Almeida, A., & Freire, C. S. R. (2019). Antimicrobial and conductive nanocellulose-based films for active and intelligent food packaging. *Nanomaterials*, *9*(7), 980. https://doi.org/10.3390/nano9070980

Vilela, C., Pinto, R. J. B., Pinto, S., Marques, P. A. A. P., Silvestre, A. J. D., & Freire, C. S. R. (2018). *Polysaccharide based hybrid materials* (1st ed.). Berlin, Germany:

Springer. https://doi.org/10.1007/978-3-030-00347-0

Vilela, C., Silvestre, A. J. D., Figueiredo, F. M. L., & Freire, C. S. R. (2019). Nanocellulose-based materials as components of polymer electrolyte fuel cells. *Journal of Materials Chemistry A*, *7*, 20045–20074. https://doi.org/10.1039/C9TA07466J

Vilela, C., Sousa, N., Pinto, R. J. B., Silvestre, A. J. D., Figueiredo, F. M. L., & Freire, C. S. R. (2017). Exploiting poly(ionic liquids) and nanocellulose for the development of bio-based anion-exchange membranes. *Biomass and Bioenergy*, *100*, 116–125. https://doi.org/10.1016/j.biombioe.2017.03.016

Wang, J., Tavakoli, J., & Tang, Y. (2019). Bacterial cellulose production, properties and applications with different culture methods – A review. *Carbohydrate Polymers*, *219*, 63–76. https://doi.org/10.1016/J.CARBPOL.2019.05.008

Wang, S., Liu, Q., Luo, Z., Wen, L., & Cen, K. (2007). Mechanism study on cellulose pyrolysis using thermogravimetric analysis coupled with infrared spectroscopy. *Frontiers of Energy and Power Engineering in China*, *1*(4), 413–419. https://doi.org/10.1007/s11708-007-0060-8

Wang, Y., Xing, M., Cao, Q., Ji, A., Liang, H., & Song, S. (2019). Biological activities of fucoidan and the factors mediating its therapeutic effects: A review of recent studies. *Marine Drugs*, *17*(3), 183. https://doi.org/10.3390/md17030183

Webber, J. L., Benbow, N. L., Krasowska, M., & Beattie, D. A. (2017). Formation and enzymatic degradation of poly-l-arginine/fucoidan multilayer films. *Colloids and Surfaces B: Biointerfaces*, *159*, 468–476. https://doi.org/10.1016/J.COLSURFB.2017.08.005

Weelden, G., Bobiński, M., Okła, K., van Weelden, W., Romano, A., & Pijnenborg, J. (2019). Fucoidan structure and activity in relation to anti-cancer mechanisms.

Marine Drugs, *17*(1), 32. https://doi.org/10.3390/md17010032

Zayed, A., & Ulber, R. (2019). Fucoidan production: Approval key challenges and opportunities. *Carbohydrate Polymers*, *211*, 289–297. https://doi.org/10.1016/J.CARBPOL.2019.01.105